A Novel Seizure Detection Method Based on the Feature Fusion of Multimodal Physiological Signals

Duanpo Wu, Jun Wei, Pierre-Paul Vidal, Danping Wang, Yixuan Yuan, *Senior Member, IEEE*, Jiuwen Cao, *Senior Member, IEEE*, and Tiejia Jiang

***Abstract*—Seizure detection is traditionally done using video/electroencephalography monitoring, but for out-of-hospital patients, this method is costly. In recent years, portable device to detect seizures gains attention. In this article, multimodal signals collected by portable devices are studied, and a seizure detection algorithm is proposed based on adaptive multibit local differential ternary pattern (MLDTP). This algorithm is used for detecting seizure period and interseizure period. Traditional local binary pattern has certain limitations in describing 1-D time-series signals. It can only describe two types of structures in signals: 1) rising structure and 2) falling structure, making the signal patterns overly monotonous and not conducive to classification tasks. To address this issue, this article introduces two additional structures, slowly rising structure and slowly falling structure, into the signal description using the MLDTP method. This method constructs multibit neighboring relationships of the signals and adaptively selects the optimal MLDTP parameters for different modalities using the Archimedes optimization algorithm (AOA). Additionally, this article extensively discusses a multimodal signal fusion strategy, mapping features of different modal signals to the same feature space through the MLDTP algorithm to achieve information complementarity. Long-term recorded data from 18 patients were collected using the wearable device Biovital P1, with 13 cases from the Children's Hospital affiliated with Children's Hospital, Zhejiang University School of Medicine, and five cases from the fourth Affiliated Hospital of Anhui Medical University. The data set underwent fivefold cross-validation, resulting in average accuracy, precision, sensitivity, and F1 score of 96.81%, 98.55%, 95.24%, and 96.87%, respectively.**

***Index Terms*—Archimedes optimization algorithm (AOA), feature fusion, local differential ternary pattern, portable device, seizure detection.**

Manuscript received 1 April 2024; revised 1 May 2024; accepted 6 May 2024. Date of publication 8 May 2024; date of current version 8 August 2024. This work was supported in part by the National Key Research and Development Program under Grant 2021YFE0100100; in part by the National Natural Science Foundation of China under Grant 62301203; in part by the Fundamental Research Funds for the Provincial Universities of Zhejiang under Grant GK239909299001-401; in part by the Joint Fund of Zhejiang Provincial Natural Science Foundation of China under Grant LBY21H090001; and in part by the NSFC–Zhejiang Integration Joint Fund under Grant U1909209. *(Corresponding author: Duanpo Wu.)*

This work involved human subjects or animals in its research. Approval of all ethical and experimental procedures and protocols was granted by the Ethic Committee of Zhejiang University under Application No. 2020-IRB-124.

Duanpo Wu is with the School of Communication Engineering and the Artificial Intelligence Institute, Hangzhou Dianzi University, Hangzhou 310018, Zhejiang, China (e-mail: wuduanpo@hdu.edu.cn).

Jun Wei is with the School of Communication Engineering, Hangzhou Dianzi University, Hangzhou 310018, China (e-mail: weijun7529@163.com).

Pierre-Paul Vidal is with the Machine Learning and I-Health International Cooperation Base of Zhejiang Province, Hangzhou Dianzi University, Hangzhou 310018, China, also with the Centre Borelli, CNRS, SSA, INSERM, Université Paris Cité, Université Paris Saclay, ENS Paris Saclay, 75006 Paris, France, and also with the Plateforme d'Etude de la Sensorimotricité, INSERM US36-CNRS2009, Université Paris Cité, 75006 Paris, France (e-mail: pierre-paul.vidal@u-paris.fr).

Danping Wang is with the Machine Learning and I-Health International Cooperation Base of Zhejiang Province, Hangzhou Dianzi University, Hangzhou 310018, China, and also with the Plateforme d'Etude de la Sensorimotricité, INSERM US36-CNRS2009, Université Paris Cité, 75006 Paris, France (e-mail: danping.wang@u-paris.fr).

Yixuan Yuan is with the Department of Electronic Engineering, The Chinese University of Hong Kong, Hong Kong (e-mail: yxyuan@ee.cuhk.edu.hk).

Jiuwen Cao is with the Machine Learning and I-Health International Cooperation Base of Zhejiang Province and the Artificial Intelligence Institute, Hangzhou Dianzi University, Hangzhou 310018, Zhejiang, China (e-mail: jwcao@hdu.edu.cn).

Tiejia Jiang is with the Children's Hospital, Zhejiang University School of Medicine, Hangzhou 310052, China (e-mail: jiangyouze@zju.edu.cn).

Digital Object Identifier 10.1109/JIOT.2024.3398418

I. Introduction

EPILEPSY is caused by paroxysmal abnormal hypersynchronous electrical activity of neurons in the brain [1] and is one of the most common psychiatric system disorders worldwide. It is characterized by recurrent seizures that are unpredictable and short duration [2]. While electroencephalography (EEG) can be used to effectively diagnose seizures, it is not the most convenient diagnostic method and is not suitable for long-term or nighttime monitoring outside the hospital [3]. New methods for seizure detection are sought by studying physiological signals generated from different modalities recorded by portable devices [4], including accelerometry (ACC), gyroscope (GYR), electromyogram (EMG), and electrodermal (EDA).

The rapid progress in multimodal seizure detection technology is marking a significant breakthrough in modern medical science [3], [5], [6]. This approach integrates an array of sensor modules, such as ACC, GYR, EMG, and EDA, to monitor and analyze patients' physiological signals. These divergent modal signals hold significant correlations with seizures [3], [6], [7], [8], [9]. ACC and GYR detect the physical movements and vibrations during seizures [7], [8], EMG captures involuntary muscle contractions throughout such events [9], and EDA indicates autonomic nervous system fluctuations [8]. Comprehensive analysis of the data harvested by wearable devices not only enhances seizure detection but also advances early warning and monitoring capabilities for epilepsy [10], [11], [12]. In the field of signal processing, there is a growing interest in researching the conversion of signals into code. The local binary pattern (LBP) method enjoys widespread adoption in the analysis of both 1-D

signals and 2-D images due to its distinct discriminatory capabilities and computationally efficient characteristics. The concept of 1-D LBP is originally introduced by Hatlani et al. and has demonstrated successful application in the detection of nonsmooth speech signals [13]. Kaya et al. [14] harnessed 1-D LBP to extract distinctive characteristics from unprocessed EEG signals, effectively showcasing its remarkable performance and minimal computational demands when dealing with nonsmooth EEG signals. Although the performance of LBP on nonsmooth signals is very objective, it is poorly adapted to noise and prone to interference. To address this problem, Khan et al. [15] proposed a hybrid method based on LBP wavelets to classify the EEG of epileptic patients. Local pattern transformation is widely applied not only in the field of electroencephalogram signals but also demonstrates unique advantages in other modalities of signal applications. Ohini and Mignotte [16] proposed classifying environmental noise using LBP combined with audio features, which has lower computational complexity compared to convolutional neural networks. Luo et al. [17] proposed a scale-selective and noise-robust extended LBP (SNELBP) descriptor, which achieves good performance between scale invariance and noise robustness. El Merabet et al. [18] proposed a novel attractive-and-repulsive center-symmetric LBP (ACS-LBP and RCS-LBP) texture descriptor, enhancing the discriminative power of LBP and its robustness to small variations. Huang et al. [19] introduced a discriminative spatiotemporal LBP (STLBP) based on integral projections, incorporating extracted shape attributes into spatiotemporal texture features. Ding et al. [20] enhanced STLBP by introducing a method that employed pixel difference vector (PDV) hashing and multiscale volume dictionary learning, effectively addressing the problem of utilizing small neighborhoods in STLBP due to high-dimensional data. Zheng et al. [21] proposed a new texture recognition model of the circular local ternary pattern (CLTP) in response to the shortcomings of LBP in texture recognition. Zhang et al. [22] proposed a seizure detection algorithm based on multibit local neighborhood difference pattern (MLNDP) and constructed a multibit neighboring relationship.

In recent years, researches on pattern recognition and classification of local pattern transformations on single modality have continued, such as Lan et al. [23], Akbal et al. [24], Al-wajih et al. [25], and Kumar et al. [26], while the performance under multimodality has not been well validated, selecting the appropriate algorithm for multimodal recognition remains a significant challenge.

In this article, we improve the LBP and MLNDP algorithms and propose a robust and efficient multibit local differential ternary pattern (MLDTP) algorithm. It is applied to multimodal seizure detection, effectively enhancing the classification performance of the model. The Archimedes optimization algorithm (AOA) is utilized to optimize the parameters of MLDTP. The algorithm is briefly described as follows. First, different modal signals are transformed into MLDTP codes and their parameters are optimized using AOA. Second, histogram features of the MLDTP codes from different modalities are extracted and feature fusion is performed. Finally, the fused features are used as input and classified using a random forest (RF) model.

The algorithm primarily provides the following three contributions to multimodal seizure detection.

1) We propose a novel multimodal pattern transformation method: MLDTP maps features of different modal signals to the same feature space.
2) We optimize the parameters of MLDTP using AOA, and the results indicate that the performance metrics of the model tend to converge after a certain number of algorithm iterations, with the greatest improvement often observed in the first iteration.
3) We extensively discuss the impact of different fusion strategies on model performance, including decision-level fusion and feature-level fusion. A comparison reveals that under the second fusion strategy, accuracy, precision, and F1 score are superior to the first strategy, while sensitivity may be higher under the first strategy in specific circumstances.

The remainder of this article is organized as follows. In Section II, the data set and the methodology used are described, including multimodal signal data acquisition, multimodal data preprocessing, MLDTP coding, feature extraction, parameter selection, feature fusion, and classification. In Section III, the performance of the experimental results is evaluated and analyzed. In Section IV, the effectiveness of the algorithm proposed in this article is discussed. In Section V, this article is summarized.

II. Data Set and Methodology

This method first preprocesses the multimodal data, encodes the preprocessed multimodal signals separately using MLDTP, and then employs the AOA algorithm to select the optimal MLDTP parameters for each modality. Next, it extracts histogram features of the MLDTP, performs feature fusion, and finally inputs these fused features into the RF classifier for seizure detection. The framework of the multimodal signal classification algorithm is shown in Fig. 1. A specific description of the details of each part is given below.

A. Multimodal Data Collection

The data of epileptic patients is collected by the Biovital P1 system, which consists of the Oppo Watch 2 and Biovital Sensor. This device enables continuous data collection for up to 12 h and features a simple wearing mechanism that does not require specialized training for users. The use of the Biovital P1 for data collection is not constrained by environmental settings nor is it disrupted by physical activity, thereby ensuring the capture of data in the most authentic scenarios. The precision of the collected data for ACC, GYR, EMG, and EDA activity are 0.0005 g, 0.61 deg/s, 12 bit, and 0.01 ms, respectively. Their sampling frequencies are 50, 50, 200, and 4 Hz, respectively. The data for this study is collected at the Children's Hospital, Zhejiang University School of Medicine (CHZU) and the fourth Affiliated Hospital

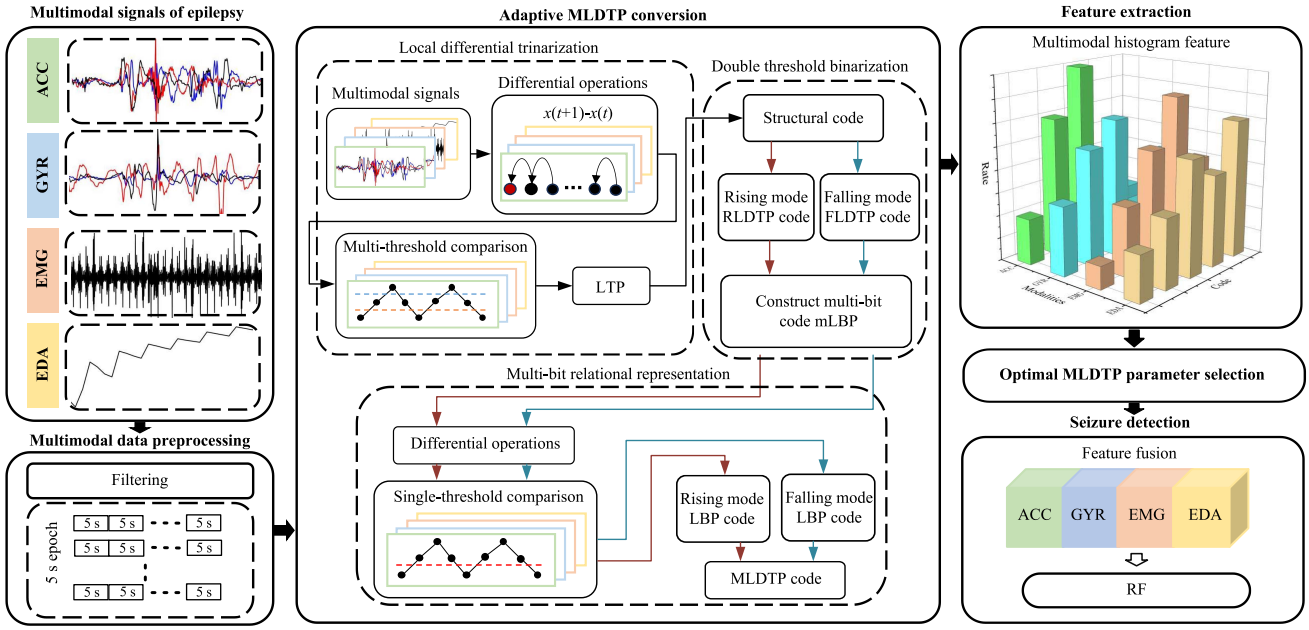

Fig. 1. Framework for classification of multimodal signals.

Fig. 2. Process of collecting data from epileptic patients.

of Anhui Medical University. The process of data collection is illustrated in Fig. 2. Between 2021 and 2024, a total of 18 patients with valid seizure data (MS_1–MS_18) are used in this study, with a total recording duration of 121.9 h. Because the duration of interseizure period data recorded for patients far exceeds that of seizure periods, this study averages the data of interseizure periods and seizure periods, truncating the interseizure period data to the same length as the seizure periods for experimental research. This study focuses on the classification of seizure period and interseizure period. The patient statistics information of gender, age, and seizures is detailed in Table I.

TABLE I
SPECIFICATIONS OF DATA SET

ID	Gender	Age	SN	SD (s)	RD (h)
MS_1	F	7Y6M	7	244	11.2
MS_2	F	2Y9M	6	21	5.1
MS_3	F	5M	2	2131	3.3
MS_4	F	7Y8M	6	1319	6.4
MS_5	F	6Y2M	2	237	6.0
MS_6	F	1Y2M	4	72	3.3
MS_7	M	7Y3M	1	33	5.4
MS_8	F	1Y4M	1	270	8.4
MS_9	M	2Y11M	5	60	3.0
MS_10	M	9Y2M	1	115	4.3
MS_11	M	5Y11M	1	51	8.7
MS_12	F	9Y	9	174	7.8
MS_13	M	11Y	1	136	7.9
MS_14	M	12Y	1	161	8.0
MS_15	F	11Y	9	154	7.4
MS_16	M	10Y	3	199	7.9
MS_17	F	7Y	5	93	8.3
MS_18	M	13Y	1	19	9.5
18 Patients	/	/	65	5489	121.9

[1] SN: Number of seizures.
[2] SD: Duration of seizures.
[3] RD: Recording duration.

B. Multimodal Data Preprocessing

The data is preprocessed to eliminate artifacts for further analysis. Band-pass filtering is performed on ACC, GYR, and EMG data at 1–24 Hz, 1–24 Hz, and 20–90 Hz, respectively, to eliminate motion artifacts and baseline noise contamination as well as high-frequency interference [27], and calculate the acceleration norms $\mathbf{F}_{\text{acc}}$ and $\mathbf{F}_{\text{gyr}}$ for ACC and GYR

$$\mathbf{F}_{\text{acc}} = \sqrt{\mathbf{acc}_x^2 + \mathbf{acc}_y^2 + \mathbf{acc}_z^2} \tag{1}$$

$$\mathbf{F}_{\text{gyr}} = \sqrt{\mathbf{gyr}_x^2 + \mathbf{gyr}_y^2 + \mathbf{gyr}_z^2} \tag{2}$$

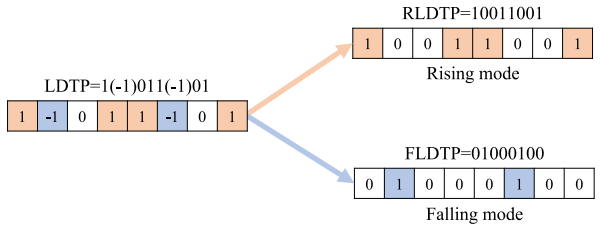

Fig. 3. Description of the two independent channels of LDTP.

where $\mathbf{acc}_x$, $\mathbf{acc}_y$, and $\mathbf{acc}_z$ are the components of acceleration on x-axis, y-axis, and z-axis, respectively. $\mathbf{gyr}_x$, $\mathbf{gyr}_y$, and $\mathbf{gyr}_z$ are the components of angular velocity on x-axis, y-axis, and z-axis, respectively. Then, multimodal data is segmented into 5 s epochs with overlap of 80%.

C. Adaptive MLDTP Conversion

MLDTP can be divided into three stages.

1) The local difference ternary pattern (LDTP) is achieved by comparing the sample values of adjacent points. It defines three types of structures in the signal: rising state, falling state, and steady state, represented by 1, −1, and 0, respectively, providing a comprehensive reflection of the signal's fluctuation characteristics.
2) Double threshold binarization is applied to encode LDTP, representing the rising mode (RLDTP) and falling mode (FLDTP), simplifying the complex ternary patterns into simple binary patterns, and simplify the LDTP code while retaining the original encoding information, as shown in Fig. 3.
3) Multibit relationship representation. After converting multimodal signals into RLDTP codes and FLDTP codes, construct multibit relationships for ascending and descending patterns separately. The correlation between different bits is enhanced while maintaining local structural features. Fig. 4 illustrates the process of converting multimodal signal into MLDTP code.

1) Local Differential Ternary Pattern: Let a segment of sampled signal be represented by $\mathbf{X}$, where x represents the value of the sampled signal

$$\mathbf{X} = \begin{bmatrix} x_1 & x_2 & \dots & x_r \end{bmatrix} \tag{3}$$

where r denotes the number of sampling points. The calculation process is consistent for different modal signals.

The differential values are obtained by performing differentiation operations on the sample points of the signal

$$d(k) = x_{k+1} - x_k \tag{4}$$

where $k \in [1, r-1]$ is the number of bits of the first-order difference matrix. Comparing $d(k)$ with the thresholds α_1 and α_2. Values greater than α_1 are mapped to 1, values less than α_2 are mapped to −1, and values between α_1 and α_2 are mapped to 0. The equation for LDTP encoding is as follows:

$$\psi(k) = \begin{cases} 1, & d(k) \geq \alpha_1 \\ 0, & \alpha_2 \leq d(k) < \alpha_1 \\ -1, & d(k) < \alpha_2 \end{cases} \tag{5}$$

where α_1 and α_2 are the determination thresholds of the LDTP code, which are adaptively optimized by AOA. The three values solved by LDTP correspond to four different microstructures. When $\psi(k) = 1$, it is defined as rising structure. When $\psi(k) = -1$, it is defined as falling structure. When $\psi(k) = 0$ ($\alpha_2 \leq d(k) < 0$), it is defined as slowly falling structure. When $\psi(k) = 0$ ($0 \leq d(k) < \alpha_1$), it is defined as slowly rising structure. Fig. 5 illustrates these various states, with the region between the blue and orange dashed lines referred to as the difference intervals c_1 and c_2, where $c_1 \in [0, \alpha_1)$ and $c_2 \in [\alpha_2, 0)$.

2) Double Threshold Binarization: Encode LDTP into RLDTP for rising mode and FLDTP for falling mode using binary threshold functions $r\psi(k)$ and $f\psi(k)$. They are then considered as two independent channels of MLDTP encoding for the input of multibit relation construction. $r\psi(k)$ and $f\psi(k)$ are calculated as follows:

$$r\psi(k) = \begin{cases} 1, & \psi(k) = 1 \\ 0, & \psi(k) \leq 0 \end{cases} \tag{6}$$

$$f\psi(k) = \begin{cases} 1, & \psi(k) = -1 \\ 0, & \psi(k) \geq 0. \end{cases} \tag{7}$$

3) Multibit Relational Representation: After calculating RLDTP and FLDTP codes, the multibit relationships of FLDTP and RLDTP codes can be converted into decimal codes using (8) and (9), respectively

$$rBP(p,n) = \sum_{j=0}^{n-1} r\psi(p) \cdot f(n,j) \tag{8}$$

$$fBP(p,n) = \sum_{j=0}^{n-1} f\psi(p) \cdot f(n,j) \tag{9}$$

where $p \in [1, r-n]$ is the pth sampling point and $n \in [1, r-1]$ is the number of bits of the first-order difference matrix used to construct the multibit code for the number of bits selected in the determination, $f(n,j)$ is an encoding equation defined as

$$f(n,j) = 2^{n-j-1} \quad \forall j \in [0, n-1]. \tag{10}$$

Differential binarization of FLDTP and RLDTP decimal codes can be expressed as

$$mRLDTP(p,n) = \begin{cases} 1, & rBP(p+1,n) - rBP(p,n) > 0 \\ 0, & \text{otherwise} \end{cases} \tag{11}$$

$$mFLDTP(p,n) = \begin{cases} 1, & fBP(p+1,n) - fBP(p,n) > 0 \\ 0, & \text{otherwise} \end{cases} \tag{12}$$

where $p \in [1, r-n-1]$. Then, the MLDTP code value can be expressed as

$$rMLDTP(i,v,n) = \sum_{j=0}^{v-1} mRLDTP(i+j,n) \cdot f(v,j) \tag{13}$$

$$fMLDTP(i,v,n) = \sum_{j=0}^{v-1} mFLDTP(i+j,n) \cdot f(v,j) \tag{14}$$

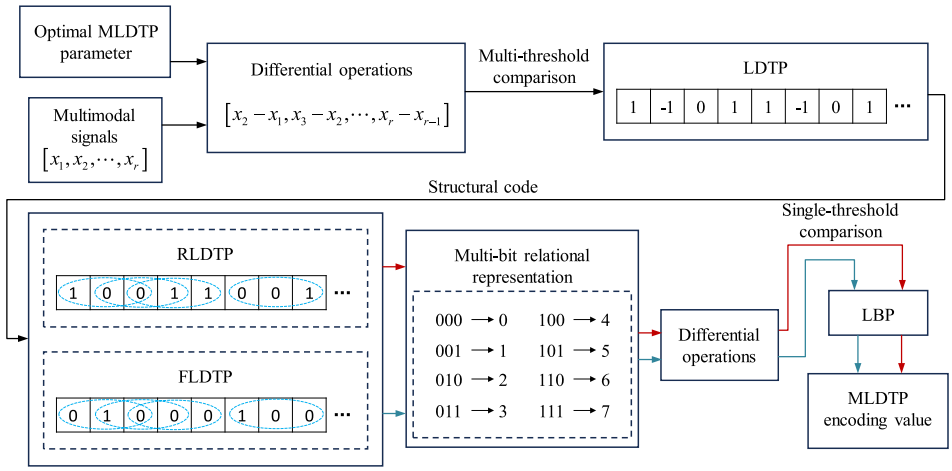

Fig. 4. Adaptive MLDTP conversion process.

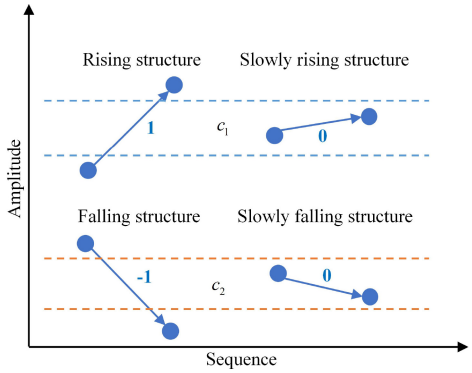

Fig. 5. Four types of signal structures.

where $i \in [1, r - v - n]$, $v \in [1, r - n - 1]$ is the number of bits of the second neighborhood difference binarization used to determine the bit code selected for constructing the MLDTP.

D. Feature Extraction

The *rMLDTP* and *fMLDTP* codes which derive from Section II-C are used to construct multibit relationship between the neighboring bits of RLDTP and FLDTP codes, respectively. Each code implies the local information of different modal signals. Therefore, it is very effective to represent the frequency of these local information by histogram features which can be calculated as follows:

$$P(c_i) = \frac{s\{c_i\}}{\sum_i s\{c_i\}}, 1 \le i \le 2^v \tag{15}$$

where c_i denotes one of the code values of the MLDTP code, and $s\{c_i\}$ denotes frequency of the code value appears in the MLDTP code.

Four different modal signals pass through MLDTP to obtain eight channel code values, half of which are in the rising mode channels and the other half are in the falling mode channels. Feature extraction is performed on the code values of these two sets of modes to reflect the local detailed features of different modal signals. The length of the feature vectors for different modes is determined by the number of multibit encoding bits v in MLDTP, with the encoding length being 2^v. By extracting histogram features, different modal signals are mapped to the same feature space. Information complementarity between different modes is achieved through feature fusion. We provide a new perspective for multimodal signal processing, especially for 1-D time-series signals like physiological electrical signals, where local fluctuation information is of significant importance for seizure detection.

E. Optimal MLDTP Parameter Selection

AOA is a population-based optimization algorithm proposed by Hashim et al. [28]. It is a versatile optimization method capable of addressing a wide range of problems across various domains. The algorithm draws inspiration from Archimedes' principle, modeling the behavior of objects submerged in fluid. In this method, the individuals of the population are submerged objects, and each individual has three attributes besides position: 1) density; 2) volume; and 3) acceleration. The acceleration of an object is adjusted by altering its density and volume, and the acceleration, together with the current position, determines the new position of the individual. Similar to other population-based metaheuristic algorithms, AOA also features an initial population search process with random volumes, densities, and accelerations. After the evaluation of the population fitness, the AOA iteration begins and continues until the number of iterations reaches the value preset by the user. In this article, the AOA algorithm is utilized to optimize the parameters α_1 and α_2 of MLDTP. The parameter settings for AOA are shown in Table II.

1) Initialization: First, we need to initialize the positions of all objects. The position O_i of the ith object is determined by

$$O_i = lb_i + \text{rand} \cdot (ub_i - lb_i), i = 1, 2, \ldots, N \tag{16}$$

where ub_i and lb_i represent the upper and lower bounds on α_1 and α_2 in MLDTP, N is the initial population size, *rand* is a random number in the range [0, 1] (including the following rand), proceed to initialize the volume and density of the ith object:

$$\text{den}_i = \text{rand} \tag{17}$$

TABLE II
AOA INITIALIZATION PARAMETERS

Parameter	Description	Value of ACC	Value of GYR	Value of EMG	Value of EDA
α_1	The range of parameter α_1 for MLDTP	[0, 1]	[0, 5]	[0, 150]	[0, 0.1]
α_2	The range of parameter α_2 for MLDTP	[-1, 0]	[-5, 0]	[-150, 0]	[-0.1, 0]
N	Population size	20	20	20	20
t_{max}	Maximum number of iterations	20	20	20	20

$$\text{vol}_i = \text{rand}. \tag{18}$$

Similarly, an object in fluid will inevitably have acceleration. Use (19) to initialize the acceleration of the ith object

$$\text{acc}_i = lb_i + \text{rand} \cdot (ub_i - lb_i). \tag{19}$$

After initialization is complete, we need to evaluate the fitness of the object and select the object with the best MLDTP parameters. The optimal properties of the object are updated simultaneously (den_{best}, vol_{best}, acc_{best}, and x_{best}).

2) Update the Density and Volume: The volume and density of the object are updated. In AOA, the volume and density of an object are not fixed and are calculated using the following formula:

$$\text{den}_i^{t+1} = \text{den}_i^t + \text{rand} \cdot \left(\text{den}_{\text{best}} - \text{den}_i^t\right) \tag{20}$$

$$\text{vol}_i^{t+1} = \text{vol}_i^t + \text{rand} \cdot \left(\text{vol}_{\text{best}} - \text{vol}_i^t\right) \tag{21}$$

where den_{best} and vol_{best} are the density and volume of the best individual in the population from the initialization to the tth iteration. t represents the current iteration of the algorithm, and $t+1$ represents the next iteration.

3) Transfer the Operator and Density Factor: In the early stages of the algorithm, collisions occur between objects, and over time, objects attempt to reach an equilibrium state. This process is implemented by the transfer operator TF. TF increases over time until it reaches 1, helping the object transition from the exploration phase to the exploitation phase

$$\text{TF} = \exp\left(\frac{t - t_{\max}}{t_{\max}}\right) \tag{22}$$

where $t_{\max}$ is the maximum number of iterations. The density decay factor helps the AOA algorithm transition from global search to local search

$$d = \exp\left(\frac{t_{\max} - t}{t_{\max}}\right) - \left(\frac{t}{t_{\max}}\right). \tag{23}$$

4) Update the Acceleration: The updating process of acceleration can be divided into two phases based on the value of the transfer operator, which are the exploration phase and the exploitation phase.

Exploration Phase: When TF $\leq$ 0.5, collisions occur between individuals, so the update method for the individual acceleration of object i is

$$\text{acc}_i^{t+1} = \frac{\text{den}_{mr} + \text{vol}_{mr} \cdot \text{acc}_{mr}}{\text{den}_i^{t+1} \cdot \text{vol}_i^{t+1}} \tag{24}$$

where den_{mr}, vol_{mr}, and acc_{mr} represent the acceleration, density, and volume of random materials, respectively.

Exploitation Phase: When TF $>$ 0.5, collisions no longer occur between individuals, and the update method for the individual acceleration of object i is

$$\text{acc}_i^{t+1} = \frac{\text{den}_{\text{best}} + \text{vol}_{\text{best}} \cdot \text{acc}_{\text{best}}}{\text{den}_i^{t+1} \cdot \text{vol}_i^{t+1}} \tag{25}$$

where acc_{best} represents the optimal acceleration from the initialization to the tth iteration.

Normalize the Acceleration: The acceleration is standardized to obtain $a_{i-\text{norm}}^{t+1}$

$$a_{i-\text{norm}}^{t+1} = u \cdot \frac{\text{acc}_i^{t+1} - \min_i\left(\text{acc}_i^{t+1}\right)}{\max_i\left(\text{acc}_i^{t+1}\right) - \min_i\left(\text{acc}_i^{t+1}\right)} + l \tag{26}$$

where u and l are set to 0.9 and 0.1, respectively, to denote the normalization range.

5) Update Position: When the object is in the exploration phase (TF $\leq$ 0.5), update the individual position using (27). When the object is in the exploitation phase (TF $>$ 0.5), update the individual position using (28)

$$x_i^{t+1} = x_i^t + C_1 \cdot rand \cdot \text{acc}_{i-\text{norm}}^{t+1} \cdot d \cdot \left(x_{\text{rand}} - x_i^t\right) \tag{27}$$

$$x_i^{t+1} = x_{\text{best}}^t + Q \cdot C_2 \cdot rand \cdot \text{acc}_{i-\text{norm}}^{t+1} \cdot d \cdot \left(H \cdot x_{\text{best}} - x_i^t\right) \tag{28}$$

$$Q = \begin{cases} +1, & \text{if } P \leq 0.5 \\ -1, & \text{if } P > 0.5 \end{cases} \tag{29}$$

where x_{best}^t represents the optimal object position in the tth iteration. x_{best} represents the optimal object position from the initialization to the tth iteration. $H = C3 \cdot \text{TF}$ is directly proportional to the transfer operator. The initial setting for H is $[0.3 \cdot C3, 1]$, and it takes a certain percentage of the optimal position. The percentage it occupies is increasing over time, and this increase in percentage is shortening the distance to the globally optimal solution. Q is a flag for changing the direction of motion. P is a random number within a specified range, defined as $P = 2 \cdot \text{rand} - C4$. The values of $C1$, $C2$, $C3$, and $C4$ are 2, 6, 1, and 0.5, respectively. It should be noted that the values of $C1$, $C2$, $C3$, and $C4$ are set according to [28].

Then, the object that obtained the optimal MLDTP parameters from the initialization to the current iteration is evaluated using the objective function, and den_{best}, vol_{best}, acc_{best}, and x_{best} are updated. When the maximum number of iterations is reached, the optimization ends, and the best MLDTP parameters are passed on to complete the subsequent seizure detection process. Fig. 6 represents the MLDTP parameter optimization process.

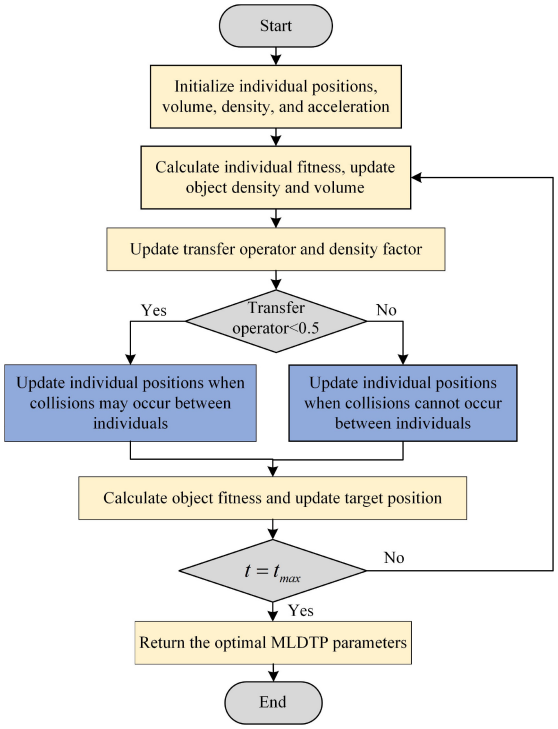

Fig. 6. Utilize AOA to optimize the parameters of the MLDTP process.

F. Seizure Detections

1) Information Fusion: This article discusses two multimodal fusion methods: 1) feature-level fusion and 2) decision-level fusion. *Feature-Level Fusion:* The MLDTP algorithm used in Section II-C maps features from different modalities to a common feature space, enhancing the accuracy of data analysis and processing. By concatenating feature matrices, information from different modal signals complements each other, addressing the issue of insufficient information from individual modalities. *Decision-Level Fusion:* A voting system based on weighted fusion is designed, where signals from each modality are individually trained to obtain different modality classification models, and corresponding weights are assigned to each model. The voting result L is determined by the decision threshold θ

$$\theta = 0.2 \cdot L_{\text{acc}} + 0.3 \cdot L_{\text{gyr}} + 0.4 \cdot L_{\text{emg}} + 0.1 \cdot L_{\text{eda}} \quad (30)$$

$$L = \begin{cases} 1, & \theta > \gamma \\ 0, & \text{otherwise} \end{cases} \quad (31)$$

where L_{acc}, L_{gyr}, L_{emg}, and L_{eda} represent the voting results of the four modalities, with 1 indicating the seizure period and 0 indicating the interseizure period. The weights for different modalities are determined based on their accuracy. The issue of the value of γ will be discussed in detail in the experimental section.

2) Random Forest: In this study, RF is used as the classification model for seizure detection. RF is an ensemble of numerous decision trees, with the final classification result being a collective decision made by these constituent trees. In the context of binary classification for seizure and interseizure periods, if the count of votes favoring seizure periods exceeds that of interseizure periods, the RF output is deemed to be in favor of seizure periods. This multimodel voting mechanism effectively mitigates the risk of overfitting while enhancing model stability [29], [30], [31]. In this study, when utilizing the RF classifier, a balance is struck between the accuracy, robustness and computational cost of the RF model, resulting in the integration of 300 decision trees.

This study assesses the classification performance of the algorithm through fivefold cross-validation. Initially, data from four different modalities are divided into five equally sized subsets using the same methodology. One of these subsets is set aside as a test set for evaluating model performance, while the remaining subsets are employed for model training. Subsequently, each subset takes its turn as the test set in a total of five iterations. Performance metrics, including accuracy, precision, sensitivity, and F1 score, are employed as evaluation criteria. Finally, the results of the five performance evaluations are averaged to provide the ultimate assessment of model performance.

III. Experiments and Results

In this section, we conduct a series of experimental analysis on a multimodal data set. First, we examine the influence of LDTP parameters passed during each iteration of AOA on model performance. Second, we discuss the correlation between the number of multibit optimized coding bits and the model performance, and verify the feasibility of the algorithm and its effectiveness by comparing the results before and after classification. Finally, we analyze and discuss the impact of two fusion strategies (decision-level fusion and feature-level fusion) on the experimental results, and compared MLDTP with existing methods based on this data set.

To assess the performance of the model, this article employs accuracy, precision, sensitivity, and F1 score as metrics, which can be calculated as follows:

$$A_c = \frac{\text{TP} + \text{TN}}{\text{TP} + \text{FN} + \text{FP} + \text{TN}} \quad (32)$$

$$P_r = \frac{\text{TP}}{\text{TP} + \text{FP}} \quad (33)$$

$$S_e = \frac{\text{TP}}{\text{TP} + \text{FN}} \quad (34)$$

$$F_1 = \frac{2 \cdot P_r \cdot S_e}{P_r + S_e} \quad (35)$$

where TP, TN, FP, and FN, respectively, represent the number of correct seizure periods detected, the number of correct interseizure periods detected, the number of incorrect seizure periods detected, and the number of incorrect interseizure periods detected during the detection process.

A. Selection of LDTP Parameters

In order to explore the effect of LDTP parameters α_1 and α_2 on model performance separately, we investigate the effect of the threshold parameters of LDTP on model performance without using multibit coding, and compare the model performance under different parameters. The default LDTP initial thresholds α_1 and α_2 are 0, and after optimizing

TABLE III
APPLICATION OF DIFFERENT ENCODING METHODS ON ACC, GYR, EMG, AND EDA

Method	ACC				GYR			
	Accuracy	Precision	Sensitivity	F1 score	Accuracy	Precision	Sensitivity	F1 score
LDTP	75.81%	71.60%	78.19%	74.75%	75.08%	71.44%	77.05%	74.13%
AOA-LDTP	80.24%	76.50%	82.69%	79.48%	81.67%	78.93%	82.69%	79.48%
AOA-MLDTP ($n=1, v=7$)	78.62%	74.84%	80.96%	77.78%	80.86%	79.02%	82.04%	80.50%
AOA-MLDTP ($n=2, v=6$)	**81.83%**	**78.60%**	84.03%	**81.23%**	**84.00%**	**81.63%**	**85.69%**	**83.61%**
AOA-MLDTP ($n=3, v=5$)	81.33%	77.11%	**84.22%**	80.51%	83.10%	80.49%	84.93%	82.65%
AOA-MLDTP ($n=4, v=4$)	79.46%	75.89%	81.73%	78.70%	81.32%	78.90%	82.91%	80.86%
Method	EMG				EDA			
	Accuracy	Precision	Sensitivity	F1 score	Accuracy	Precision	Sensitivity	F1 score
LDTP	86.80%	88.36%	85.70%	87.00%	68.51%	69.83%	68.03%	68.92%
AOA-LDTP	91.88%	93.84%	90.30%	92.04%	77.66%	71.97%	**81.20%**	**76.31%**
AOA-MLDTP ($n=1, v=7$)	92.63%	94.49%	91.09%	92.76%	76.31%	**74.31%**	77.41%	75.83%
AOA-MLDTP ($n=2, v=6$)	**94.39%**	**96.15%**	**92.88%**	**94.49%**	**78.82%**	73.40%	78.80%	76.00%
AOA-MLDTP ($n=3, v=5$)	93.91%	96.07%	92.08%	94.04%	76.71%	73.33%	78.65%	75.89%
AOA-MLDTP ($n=4, v=4$)	92.31%	94.31%	90.69%	92.46%	76.34%	72.25%	78.68%	75.33%

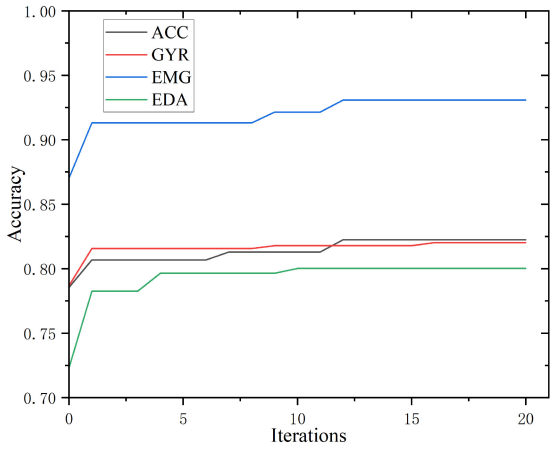

Fig. 7. AOA-LDTP performance optimization curve.

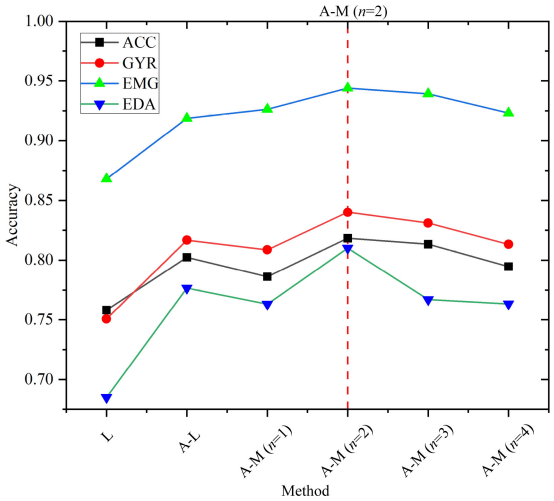

Fig. 8. Classification accuracy of the model under different encoding methods, where L, A-L, and A-M, respectively, represent LDTP, AOA-LDTP, and AOA-MLDTP (when $n = 2$, the accuracy of all modalities is at its highest).

the model performance for the LDTP thresholds for the four modalities, the curve of model performance with the number of iterations is shown in Fig. 7. When using AOA to optimize LDTP parameters, we first initialize AOA with a population size of 20 and a population dimension of 2. Next, we specify different LDTP threshold ranges for different modalities. The LDTP parameter ranges for different modal signals are shown in Table II. From the accuracy change curve of the model prediction results, it is evident that selecting appropriate LDTP parameters is crucial for improving the classification performance of the model.

B. Performance Analysis of MLDTP

To study the impact of different bit numbers on MLDTP, we discuss MLDTP encoding bit numbers in Table III (individually for ACC, GYR, EMG, and EDA). From LDTP to AOA-MLDTP (multibit encoding with $n = 4$), the accuracy, precision, sensitivity, and F1 score for each modality are listed. We find that the accuracy for all modalities reaches the optimum when the encoding bit number in MLDTP is $n = 2$. Therefore, we select $n = 2$ as the optimal MLDTP parameter. The classification accuracy under different methods is shown in Fig. 8.

In order to verify that the AOA algorithm can effectively enhance the performance of the MLDTP algorithm, we conduct multibit encoding on the unoptimized LDTP. The comparison results are shown in Fig. 9. Through the comparison, we observed that the performance of AOA-MLDTP is superior to MLDTP. Therefore, we can infer that optimizing LDTP parameters is necessary for improving model performance. Additionally, it is evident that multibit encoding, whether in MLDTP or AOA-MLDTP, consistently enhances model performance.

C. Performance Analysis of Decision-Level Fusion and Feature-Level Fusion

In this section, we extensively discuss decision-level fusion and feature-level fusion, further analyzing the impact of

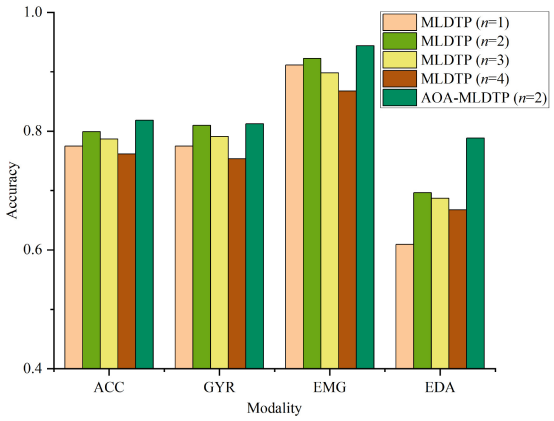

Fig. 9. Comparing the use of multibit encoding alone versus using both AOA and multibit encoding simultaneously.

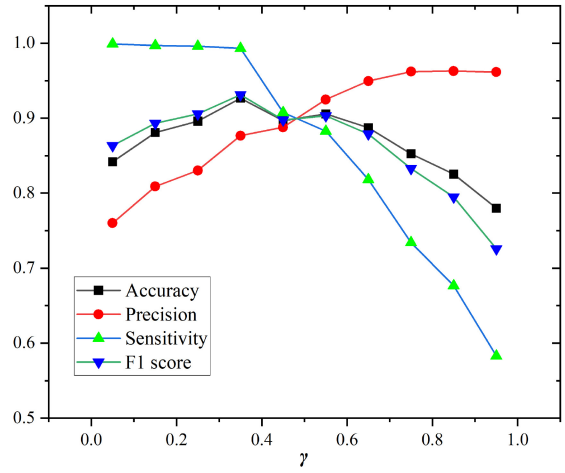

Fig. 10. Curve of classifier performance with varying threshold γ in a voting system.

TABLE IV
PERFORMANCE ANALYSIS UNDER DIFFERENT SENSITIVITIES OF VOTING SYSTEM

Threshold (γ)	Accuracy	Precision	Sensitivity	F1 score
0.05	84.18%	76.00%	**99.91%**	86.33%
0.15	88.08%	80.89%	99.70%	89.32%
0.25	89.60%	83.02%	99.58%	90.55%
0.35	**92.66%**	87.66%	99.30%	**93.12%**
0.45	89.65%	88.79%	90.76%	89.76%
0.55	90.55%	92.49%	88.26%	90.33%
0.65	88.73%	94.94%	81.82%	87.89%
0.75	85.25%	96.21%	73.40%	83.27%
0.85	82.52%	**96.28%**	67.66%	79.47%
0.95	77.98%	96.15%	58.30%	72.58%

fusion strategies on seizure detection. The optimal MLDTP parameters obtained in Sections III-A and III-B are used for the feature extraction part of this section.

Decision-Level Fusion: We employ a fusion strategy based on weighted voting (30) and (31), setting weights for seizure detection accuracy from different modalities (ACC, GYR, EMG, and EDA with weights of 0.2, 0.3, 0.4, and 0.1, respectively), and discuss seizure detection scenarios at different threshold values γ, as shown in Table IV.

By observing the relationship between threshold γ and model performance, we notice that as the threshold gradually increases, the accuracy, sensitivity, and F1 score of the model all show a decreasing trend, with only precision showing continuous improvement. The reason for this phenomenon is that a lower threshold allows fewer votes or lower weighted votes to determine whether a seizure occurs, leading to an increase in model sensitivity. In the case of $\gamma = 0.05$, only any one modality signal is required to detect seizures. On the other hand, a higher threshold requires more votes or higher weighted votes to determine a seizure, resulting in a decrease in sensitivity but an increase in precision. In the case of $\gamma = 0.95$, all modalities is required to detect a seizure for the system to classify the result as a seizure event. In some scenarios where high sensitivity is required for detecting seizures, this can be achieved by setting appropriate thresholds. The analysis results are illustrated in Fig. 10.

Feature-Level Fusion: In this section, we focus on discussing the impact of different modality combinations on seizure detection. In Sections III-A and III-B, we map signals from different modalities to the same feature space. Now, we concatenate signals from different modalities. The results are presented in Table V. From Table V, we observe that when integrating information from four modalities ACC, GYR, EMG, and EDA, the model achieves accuracy, sensitivity, and F1 scores of 96.81%, 95.24%, and 96.87%, respectively, which are the highest among all fusion methods. This indicates that integrating information from multiple modalities can leverage complementary information between different modalities, thereby enhancing the classification performance of the model.

In Table VI, we compare our method with conventional time–frequency domain feature extraction and MLNDP methods using the same data set. Compared to the other two methods, our method improves the accuracy, precision, sensitivity, and F1 score by 2.54%–3.65%, 0.95%, 3.73%–7.08%, and 2.42%–6.87%, respectively. Therefore, our proposed seizure detection algorithm based on MLDTP is indeed effective in the application of multimodal signals, providing new insights for multimodal seizure detection.

IV. DISCUSSION

In Table VI, we compare our method with other methods. When using conventional time–frequency feature extraction methods, the accuracy, sensitivity, and F1 score of seizure detection are 93.16%, 88.16%, and 90.00%, respectively. When using the MLNDP proposed in 2023, the accuracy, precision, sensitivity, and F2 score of seizure detection are 94.27%, 97.60%, 91.51%, and 94.45%, respectively. Compared to the above two methods, AOA-MLDTP achieves the best performance in all performance metrics, with an accuracy, precision, sensitivity, and F1 score of 96.81%, 98.55%, 95.24%, and 96.87% for seizure detection. This indicates that the application of AOA-MLDTP on multimodal signals is indeed effective. Local pattern encoding has achieved positive results in the classification performance of signals across different modalities, thanks to its effectiveness in describing

TABLE V
PERFORMANCE ANALYSIS OF MODEL CLASSIFICATION UNDER DIFFERENT FUSION STRATEGIES

Number	ACC	GYR	EMG	EDA	Accuracy	Precision	Sensitivity	F1 score
1	✓	×	×	×	81.83%	78.60%	84.03%	81.23%
2	×	✓	×	×	84.00%	81.63%	85.69%	83.61%
3	×	×	✓	×	94.39%	96.15%	92.88%	94.49%
4	×	×	×	✓	78.82%	73.40%	78.80%	76.00%
5	✓	✓	×	×	87.00%	85.86%	87.87%	86.85%
6	✓	×	✓	×	95.69%	98.11%	93.59%	95.79%
7	✓	×	×	✓	84.78%	83.24%	85.89%	84.55%
8	×	✓	✓	×	96.37%	97.64%	95.22%	96.42%
9	×	✓	×	✓	86.13%	82.71%	88.80%	85.65%
10	×	×	✓	✓	95.69%	98.46%	93.30%	95.81%
11	✓	✓	✓	×	96.45%	98.16%	94.92%	96.51%
12	✓	✓	×	✓	88.44%	86.46%	90.01%	88.20%
13	✓	×	✓	✓	96.19%	**98.67%**	94.02%	96.29%
14	×	✓	✓	✓	96.72%	98.53%	95.09%	96.78%
15	✓	✓	✓	✓	**96.81%**	98.55%	**95.24%**	**96.87%**

TABLE VI
COMPARISON OF DIFFERENT FEATURE EXTRACTION METHODS

Modalities	Methodology	Classifier	Accuracy	Precision	Sensitivity	F1 score
ACC, GYR, EMG, EDA	Conventional time-domain features and frequency-domain features [31]	KNN	93.16%	-	88.16%	90.00%
ACC, GYR, EMG, EDA	MLNDP [22]	RF	94.27%	97.60%	91.51%	94.45%
ACC, GYR, EMG, EDA	AOA-MLDTP	RF	**96.81%**	**98.55%**	**95.24%**	**96.87%**

the local texture features of signals. For 1-D time-series signals, the first-order difference between adjacent sample points can describe the signal's trend at the current moment. Each MLDTP code value obtained using the MLDTP method can correspond to a specific inherent change pattern of the signal within that time period. Traditional binary encoding can only describe two types of structures in signals rising and falling, which is not conducive to a comprehensive description of a signal segment. To address this, MLDTP encoding introduces two additional structures for signals: 1) slowly rising structure and 2) slowly falling structure (as shown in Fig. 5), containing richer local texture features. By statistically analyzing the frequencies of different code words, the overall change pattern of the signal within that time period can be reflected. Compared to the cumbersome process of calculating multimodal signal features in conventional methods, the MLDTP algorithm simplifies the feature extraction process while ensuring performance. Furthermore, compared to traditional local pattern transformation algorithms, it achieves better results across different modalities.

V. CONCLUSION

In this article, we propose a novel multimodal seizure detection algorithm. By extracting the MLDTP histogram features, we map features from different modalities to the same feature space. We optimize the MLDTP parameters separately for different modalities to achieve the best seizure detection performance on individual modalities. Through feature fusion, we enhance information complementarity between different modalities, effectively improving the precision and sensitivity of seizure detection.

The MLDTP algorithm proposed in this article improves upon the traditional local pattern transformation method by introducing a dual-channel encoding mode that includes both rising and falling patterns. The advantage of dual-channel encoding over traditional encoding is its ability to incorporate more local signal fluctuation information. Additionally, we construct neighborhood multibit relationships for both rising and falling patterns, enriching local features while increasing temporal correlations. The algorithm is validated on a data set containing data from 18 epilepsy patients, achieving accuracy, precision, sensitivity, and F1 score of 96.81%, 98.55%, 95.24%, and 96.87%, respectively. Compared to other algorithms, this algorithm demonstrates better classification performance on multimodal signals. This study is conducted under the condition of balanced positive and negative sample sizes. In the future, we will consider adding more samples and choose one of g-mean, Matthews correlation coefficient (MCC), or kappa as the performance metric for optimizing the parameters of the MLDTP algorithm, in order to address the optimization error issue caused by the imbalance of positive and negative sample data. We will further refine our device and algorithms, transmit data through Bluetooth and WiFi, and develop it into an IoT product, allowing for its extensive application in outpatient medical settings.

REFERENCES

[1] A. Shoeibi et al., "A comprehensive comparison of handcrafted features and convolutional autoencoders for epileptic seizures detection in EEG signals," *Expert Syst. Appl.*, vol. 163, Jan. 2021, Art. no. 113788.

[2] T. Kim et al., "Epileptic seizure detection and experimental treatment: A review," *Front. Neurol.*, vol. 11, p. 701, Jul. 2020.
[3] F. S. Leijten et al., "Multimodal seizure detection: A review," *Epilepsia*, vol. 59, pp. 42–47, Jun. 2018.
[4] B. H. Brinkmann et al., "Seizure diaries and forecasting with wearables: Epilepsy monitoring outside the clinic," *Front. Neurol.*, vol. 12, Jul. 2021, Art. no. 690404.
[5] S. Jahan et al., "AI-based epileptic seizure detection and prediction in Internet of healthcare things: A systematic review," *IEEE Access*, vol. 11, pp. 30690–30725, Mar. 2023.
[6] J. Li and Q. Wang, "Multi-modal bioelectrical signal fusion analysis based on different acquisition devices and scene settings: Overview, challenges, and novel orientation," *Inf. Fusion*, vol. 79, pp. 229–247, Mar. 2022.
[7] M. Milošević et al., "Automated detection of tonic–clonic seizures using 3-D accelerometry and surface electromyography in pediatric patients," *IEEE J. Biomed. Health Informat.*, vol. 20, no. 5, pp. 1333–1341, Sep. 2015.
[8] F. Onorati et al., "Multicenter clinical assessment of improved wearable multimodal convulsive seizure detectors," *Epilepsia*, vol. 58, no. 11, pp. 1870–1879, Oct. 2017.
[9] J. J. Halford et al., "Detection of generalized tonic–clonic seizures using surface electromyographic monitoring," *Epilepsia*, vol. 58, no. 11, pp. 1861–1869, Oct. 2017.
[10] A. V. de Vel et al., "Non-EEG seizure detection systems and potential SUDEP prevention: State of the art: Review and update," *Seizure*, vol. 41, pp. 141–153, Oct. 2016.
[11] C. Jory, R. Shankar, D. Coker, B. McLean, J. Hanna, and C. Newman, "Safe and sound? A systematic literature review of seizure detection methods for personal use," *Seizure*, vol. 36, pp. 4–15, Mar. 2016.
[12] J. van Andel, R. D. Thijs, A. de Weerd, J. Arends, and F. Leijten, "Non-EEG based ambulatory seizure detection designed for home use: What is available and how will it influence epilepsy care?" *Epilepsy Behav.*, vol. 57, pp. 82–89, Apr. 2016.
[13] Y. Li, H. Tang, W. Xie, and W. Luo, "Multidimensional local binary pattern for hyperspectral image classification," *IEEE Trans. Geosci. Remote Sens.*, vol. 60, Apr. 2021, Art. no. 5505113.
[14] Y. Kaya, M. Uyar, R. Tekin, and S. Yildirim, "1D-local binary pattern based feature extraction for classification of epileptic EEG signals," *Appl. Math. Comput.*, vol. 243, pp. 209–219, Sep. 2014.
[15] K. A. Khan, P. P. Shanir, Y. U. Khan, and O. Farooq, "A hybrid local binary pattern and wavelets based approach for EEG classification for diagnosing epilepsy," *Expert Syst. Appl.*, vol. 140, Feb. 2020, Art. no. 112895.
[16] O. K. Toffa and M. Mignotte, "Environmental sound classification using local binary pattern and audio features collaboration," *IEEE Trans. Multimedia*, vol. 23, no. 1, pp. 3978–3985, Nov. 2020.
[17] Q. Luo, J. Su, C. Yang, O. Silven, and L. Liu, "Scale-selective and noise-robust extended local binary pattern for texture classification," *Pattern Recognit.*, vol. 132, Dec. 2022, Art. no. 108901.
[18] Y. El Merabet, Y. Ruichek, and A. El Idrissi, "Attractive-and-repulsive center-symmetric local binary patterns for texture classification," *Eng. Appl. Artif. Intell.*, vol. 78, pp. 158–172, Feb. 2019.
[19] X. Huang, S.-J. Wang, X. Liu, G. Zhao, X. Feng, and M. Pietikäinen, "Discriminative spatiotemporal local binary pattern with revisited integral projection for spontaneous facial micro-expression recognition," *IEEE Trans. Affect. Comput.*, vol. 10, no. 1, pp. 32–47, Jan.–Mar. 2019.
[20] R. Ding, J. Ren, H. Yu, and J. Li, "Dynamic texture recognition using PDV hashing and dictionary learning on multi-scale volume local binary pattern," in *Proc. IEEE Int. Conf. Acoust., Speech Signal Process. (ICASSP)*, May 2022, pp. 1840–1844.
[21] Z. Zheng et al., "Circumferential local ternary pattern: New and efficient feature descriptors for anti-counterfeiting pattern identification," *IEEE Trans. Inf. Forensics Security*, vol. 17, pp. 970–981, Feb. 2022.
[22] W. Zhang, D. Wu, J. Cao, L. Jiang, and T. Jiang, "Multi-bit local neighborhood difference pattern optimization for seizure detection of west syndrome EEG signals," *IEEE Sensors J.*, vol. 23, no. 19, pp. 22693–22703, Oct. 2023.
[23] S. Lan, H. Fan, S. Hu, X. Ren, X. Liao, and Z. Pan, "An edge-located uniform pattern recovery mechanism using statistical feature-based optimal center pixel selection strategy for local binary pattern," *Expert Syst. Appl.*, vol. 221, Jul. 2023, Art. no. 119763.
[24] E. Akbal, P. D. Barua, S. Dogan, T. Tuncer, and U. R. Acharya, "Explainable automated anuran sound classification using improved one-dimensional local binary pattern and tunable Q wavelet transform techniques," *Expert Syst. Appl.*, vol. 225, Sep. 2023, Art. no. 120089.
[25] E. Al-Wajih and R. Ghazali, "Threshold center-symmetric local binary convolutional neural networks for bilingual handwritten digit recognition," *Knowl.-Based Syst.*, vol. 259, Jan. 2023, Art. no. 110079.
[26] T. S. Kumar, K. N. V. P. S. Rajesh, S. Maheswari, V. Kanhangad, and U. R. Acharya, "Automated schizophrenia detection using local descriptors with EEG signals," *Eng. Appl. Artif. Intell.*, vol. 117, Jan. 2023, Art. no. 105602.
[27] K. Cuppens et al., "Accelerometry-based home monitoring for detection of nocturnal hypermotor seizures based on novelty detection," *IEEE J. Biomed. Health Inform.*, vol. 18, no. 3, pp. 1026–1033, May 2014.
[28] F. A. Hashim, K. Hussain, E. H. Houssein, M. S. Mabrouk, and W. Al-Atabany, "Archimedes optimization algorithm: A new meta-heuristic algorithm for solving optimization problems," *Appl. Intell.*, vol. 51, pp. 1531–1551, Mar. 2021.
[29] J. L. Speiser, M. E. Miller, J. Tooze, and E. Ip, "A comparison of random forest variable selection methods for classification prediction modeling," *Expert Syst. Appl.*, vol. 134, pp. 93–101, Nov. 2019.
[30] R. R. Fernández, I. M. De Diego, V. Aceña, A. Fernández-Isabel, and J. M. Moguerza, "Random forest explainability using counterfactual sets," *Inf. Fusion*, vol. 63, pp. 196–207, Nov. 2020.
[31] W. Gao and Z.-H. Zhou, "Towards convergence rate analysis of random forests for classification," in *Proc. 34th Adv. Neural Inf. Process. Syst.*, 2020, pp. 9300–9311.
[32] Y. Ge et al., "Epilepsy analysis with portable device based multi-modal physiological signals," in *Proc. 38th Youth Acad. Annu. Conf. Chin. Assoc. Autom. (YAC)*, 2023, pp. 154–159.

Duanpo Wu received the B.S. degree from the College of Electronics and Information, Hangzhou Dianzi University, Hangzhou, China, in 2009, and the Ph.D. degree from the College of Information Science and Electronic Engineering, Zhejiang University, Hangzhou, in 2014.

Since 2022, he has been an Associate Professor with Hangzhou Dianzi University. His research interests include intelligent signal processing, biological data analysis, and machine learning.

Jun Wei is currently pursuing the master's degree with Hangzhou Dianzi University, Hangzhou, China.

His research interests include the signal processing and machine learning applications in the field of seizure detection.

Pierre-Paul Vidal received the M.D. degree in 1978 and the Scientific Ph.D. degree from Univercité Paris in 1986.

He is the Director of Research Emeritus with the National Center for Scientific Research (CNRS), Paris, France. He served as the Head of the Laboratory, CNRS from 1990 to 2020. He is also the Scientific Director of the Platform for the Study of Sensorimotricity with Université Paris Cité, Paris. He also serves as a Professor in Portugal, Spain, and China. Under his leadership, numerous achievements in the fields of neurorehabilitation treatment equipment, electric pulse sterilization equipment, and smart health evaluation and monitoring systems have been successfully implemented in hospitals in both China and France for the fragility prevention.

Danping Wang received the engineering and Master of Science degrees from the Northeast Institute of Heavy Machinery, Qiqiaer, China, in 1982 and 1988, respectively, and the Ph.D. degree from the University Technologie de Compiègne, Compiègne, France, in 1999.

Since 2006, she has been working as a Research Engineer with Université Paris Cité, Paris, France. Her research focuses on human behavior in neuroscience and biomechanics.

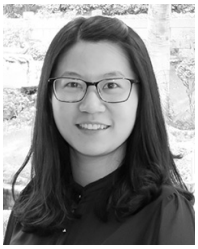

Yixuan Yuan (Senior Member, IEEE) received the B.S. degree from the College of Information Countermeasure, Northwestern Polytechnical University, Xi'an, China, in 2010, and the Ph.D. degree from the College of Biomedical Engineering, The Chinese University of Hong Kong, Hong Kong, China, in 2016.

Since 2022, she has been an Assistant Professor with The Chinese University of Hong Kong. Her research interests include biomedical image analysis and deep learning.

Jiuwen Cao (Senior Member, IEEE) received the B.Sc. and M.Sc. degrees from the School of Applied Mathematics, University of Electronic Science and Technology of China, Chengdu, China, in 2005 and 2008, respectively, and the Ph.D. degree from the School of Electrical and Electronic Engineering, Nanyang Technological University (NTU), Singapore, in 2013.

From 2012 to 2013, he was a Research Fellow with NTU. He is a Full Professor and the Dean of the School of Automation, Hangzhou Dianzi University, Hangzhou, China. His main research interests include machine learning, neural networks, and intelligent signal processing.

Dr. Cao is serving as an Associate Editor of IEEE TRANSACTIONS ON CIRCUITS AND SYSTEMS—PART I: REGULAR PAPER, *Journal of the Franklin Institute*, *Multidimensional Systems and Signal Processing*, *Memetic Computing*, and *Military Medical Research*.

Tiejia Jiang received the B.S. degree from the Department of Clinical Medicine, Wenzhou Medical University, Wenzhou, China, in 2008, and the M.S. degree in pediatrics from Zhejiang University, Hangzhou, China, in 2017.

He is currently the Deputy Chief Physician with the Children's Hospital, Zhejiang University School of Medicine. He is mainly engaged in electrophysiological signal analysis and research of various children's neurological diseases.